# Surface Pressure Measurements on a Transonic Spinning Projectile

M.C. Miller*
*Chemical Research and Development Center, U.S. Army Armament, Munitions and Chemical Command*
*Aberdeen Proving Ground, Maryland*

**The aerodynamic surface pressures on a spinning projectile were experimentally obtained during transonic wind tunnel tests employing a novel model design and instrumentation arrangement. A series of remotely controlled pressure taps located in the nonspinning inner portion of the wind tunnel model detected the surface pressures through vent holes in the spinning outer portion. Data were obtained at spin rates of 0 and 82 Hz for angles of attack of 0, 4, and 10 deg. Testing was conducted at a Mach number of 0.94 and Reynolds number of $4\times10^6$ per foot. The results illustrate the large circumferential pressure variation over the boattail region as well as the nonlinear effect of angle of attack. The integrated pressure data indicate not only the total Magnus force and moment coefficients for the model, but also the individual contributions of the various body components.**

## Nomenclature

$C_N$ = normal force coefficient $N/qS$
$C_{N_i}$ = local normal force coefficient, $2d_i\sin\Delta\phi \sum_{j=1}^{360/\Delta\phi} C_{p_j}\sin\phi_j/\pi d^2$
$C_{N_\alpha}$ = $\partial C_N/\partial\alpha$
$C_m$ = pitching moment coefficient, $PM/qSd$
$C_{m_\alpha}$ = $\partial C_m/\partial\alpha$
$C_n$ = yawing moment coefficient, $YM/qSd$
$C_{n_p}$ = $\partial C_n/\partial\hat{p}$
$C_p$ = pressure coefficient, $(P-P_\infty)/q$
$C_Y$ = side force coefficient, $SF/qS$
$C_{y_p}$ = $\partial C_Y/\partial\hat{p}$
$C_{Y_i}$ = local side force coefficient, $2d_i\sin\Delta\phi \sum_{j=i}^{360/\Delta\phi} C_{p_j}\cos\phi_j/\pi d^2$
$d$ = model reference diameter
$L$ = projectile length
$M$ = Mach number
$N$ = normal force
$P$ = surface pressure
$P_\infty$ = freestream static pressure
$PM$ = pitching moment
$P$ = spin rate
$\hat{p}$ = tip speed ratio, $pd/2V$
$q$ = dynamic pressure, $\rho V^2/2$
$R_d$ = Reynolds number, $V/\nu$
$S$ = reference area, $\pi d^2/4$
$SF$ = side force
$t$ = time
$V$ = total freestream velocity
$x,y,z$ = body axes
$YM$ = yawing moment
$Z$ = distance along model from nose
$Z_{cg}$ = longitudinal location of reference center of gravity from nose
$Z_{CP}/L$ = normal force center of pressure location from nose, $0.625-0.1782\ (C_{M_\alpha}/C_{N_\alpha})$
$Z_{CP}/L$ (Magnus) = Magnus force center of pressure location from nose, $0.625+0.1782\ (C_{n_p}/C_{Y_p})$
$\alpha$ = angle of attack
$\Delta P$ = $P-P_\infty$
$\Delta\phi$ = circumferential increment
$\nu$ = air kinematic viscosity
$\rho$ = air density
$\phi$ = circumferential location

*Subscripts*

$i$ = value at location $Z_i$
$j$ = value at location $\phi_j$

Presented as Paper 83-1838 at the AIAA Applied Aerodynamics Conference, Danvers, Mass., July 13-15, 1983; received July 29, 1983; revision received Nov. 28, 1983. This paper is declared a work of the U.S. Government and therefore is in the public domain.

*Chief, Aerodynamics Research and Concepts Assistance Section, Physics Branch, Research Division. Member AIAA.

## Introduction

A SPINNING projectile in flight experiences aerodynamic surface pressures which have led to the so-called Magnus effect. This aerodynamic phenomenon, due to the combination of projectile spin and angle of attack, produces forces and associated moments which have resulted in flight instabilities for several military projectiles.[1,2,3] Although the Magnus force is only a tenth to a hundredth of the normal force, it can have a large detrimental influence on range and accuracy.[4] A concerted effort has been underway to investigate the fundamental Magnus phenomena experimentally and to develop theoretical models and analytical techniques to describe the effect.

This paper presents wind tunnel measurements of the aerodynamic surface pressures on a spinning model of an artillery projectile at a transonic Mach number. The model consisted of a secant ogive, cylinder, and boattail with and without a rotating band. The 8-in.-diam, 5.5-caliber length model was tested in the NASA Ames 14-Foot Transonic Wind Tunnel. Pressures were measured at several longitudinal locations on the model, with emphasis on the cylindrical and boattail sections. The model was tested at angles of atack of 0, 4, and 10 deg and spin rates of 0 and 4,900 rpm. All testing was done at a Mach number of 0.94. The 0.94 test Mach number represents the critical Mach number for this projectile where the projectile possesses the maximum destabilizing aerodynamic effects. At this transonic condition, two separate shock waves are present, one near the ogive/cylinder junction and the other near the cylinder/boattail junction.

The resultant combination of subsonic and supersonic flow produce a highly complex surface pressure distribution. Angles of attack of 4 and 10 deg result in attached and separated flow, respectively, over the boattail region of the model. The spin rate of 4,900 rpm represents a tip speed ratio of 0.162, corresponding to a Mach number 0.94 muzzle velocity condition. Finally, the influence of the rotating band on the Magnus surface pressures in the transonic speed regime is of current concern.

The projectile configuration, model scale, and test conditions were identical to a series of wind tunnel tests conducted at the NASA Langley 8-Foot Transonic Wind Tunnel.[5] During those tests, the aerodynamic forces and moments and boundary layer velocity profiles were obtained on both spinning and nonspinning models. The aerodynamic surface pressures were also measured, but only for the nonspinning condition. The test described in this paper is intended to extend the experimental data base for this projectile configuration[6] and to support theoretical and numerical analyses.[7] In addition, the test demonstrated the use of a new experimental method to obtain the surface pressure data.

The method is based on an unconventional model design and instrumentation arrangement. The model is composed of two parts. A nonspinning inner portion contains instrumentation which detects the surface pressure through a series of vent holes in the spinning outer portion, the pressure being retained for measurement by means of a sliding seal arrangement.[8] The value of this testing method has been demonstrated with a simple spinning circular cylinder in crossflow which verified the basic concept.[9] A second major series of tests involved the measurements of the surface pressure on a spinning Magnus autorotor[10] which extended the testing method to bodies having irregular surface features and an unsteady, periodic flow field. Other studies investigated improvements to the critical sliding seal units. This work evolved a magnetic fluid seal,[11] a miniature sized seal, and a remotely selectable pneumatic seal; all intended to increase the versatility and accuracy of the testing method. These efforts prepared the way for the most recent application involving the surface pressure measurements on a spinning projectile in transonic flow.

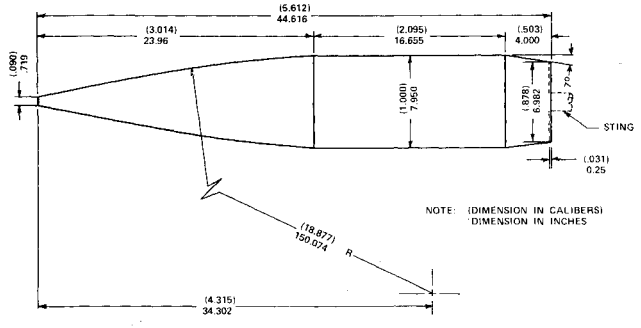


**Fig. 1 Wind tunnel model external configuration.**

## Model Description

The model external configuration is shown in Fig. 1 and was composed of a three-caliber secant ogive nose, a two-caliber cylindrical section, and a 7-deg, 0.5-caliber boattail. The model is a 130% scale 155 mm artillery projectile identical to the model used in the Langley test.[5]

A schematic drawing of the model internal arrangement is shown in Fig. 2. The model consisted of an aluminum core containing the spin motor, pressure taps, and scanivalve mechanism. The model core was fixed with respect to the model sting. The steel outer contour shell of the projectile was attached to the core by means of front and rear bearings and connected to the spin motor through an axial drive shaft at the nose. A set of four vent holes at 90-deg circumferential intervals was located through the shell at each of 20 longitudinal stations along the model. These 0.0625-in.-diam vent holes coincided with 20 pressure taps contained in the outer surface of the core section. Only two taps are shown for clarity.

Two scanivalves located in the core were used as switching devices to allow the remote selection and engagement of the pressure taps. The scanivalves were simultaneously driven by a common index/drive unit also located in the model core. Once scanivalve directed pneumatic air to a particular pressure tap seal unit to force it outward against the inner surface of the spinning shell. Concurrently, the other scanivalve directed the surface pressure being measured by that tap out through the sting to the pressure transducer and associated recording equipment located outside the tunnel.

The gap between the face of the pressure tap seal unit and the inner surface of the shell was sealed by means of an O-ring located on the outer face of the seal unit. The cavity created within the seal unit was open to the pressure acting on the outside surface of the shell when the vent hole was aligned with the tap as illustrated in Fig. 3. Once the vent hole in the spinning shell rotated past this aligned position, the seal caused the cavity to retain the pressure. The cavity eventually assumed a constant pressure with time equal to the pressure acting on the surface of the spinning model at that particular circumferential location. Details of a pressure tap seal unit are shown in Fig. 4. The outer surface of each seal unit was contoured to match the radius of the inner shell surface at that location. The 0.5-in.-diam O-rings were composed of lubricant impregnated rubber and were retained in the circular groove of the seal block by high viscosity silicone oil. Pressure measurements at various points on the surface of the spinning body were obtained by positioning the core and the attached tap to different roll attitudes relative to the angle-of-attack plane. A remotely settable roll head located between the model sting and the tunnel angle-of-attack sector allowed the model core to be sequentially set to the various roll orientations.

The steel shell was made up of two parts. The forward part included the ogive and most of the cylindrical section. The aft part included the boattail and the portion of the cylindrical section in the area of the rotating band. The band, which represented a post-fired condition, was machined directly into

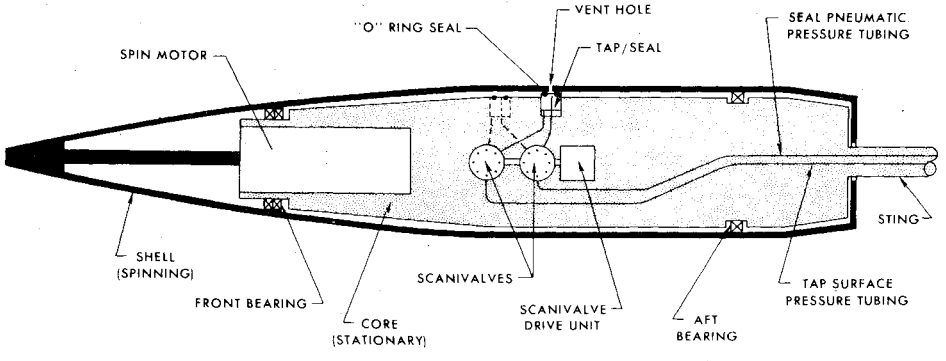


**Fig. 2 Wind tunnel model internal configuration.**

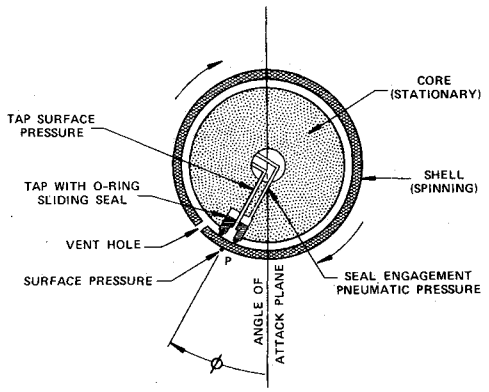


**Fig. 3 Surface pressure measurement technique.**

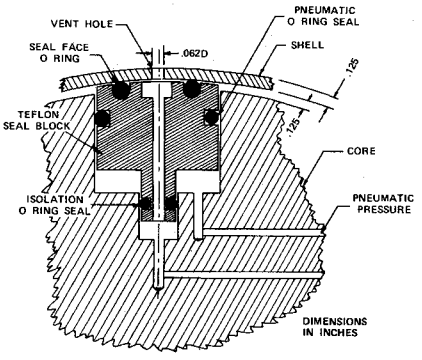


**Fig. 4 Pressure tap sliding seal.**

the aft-shell section. The model could be tested with or without the rotating band by simply changing the aft part of the shell. Vent holes were also located on the rotating band protrusions and indentations allowing measurements at these positions. The model included an enclosed base similar to the actual projectile.

The pressure tap longitudinal locations for the 20 vent holes are defined in Fig. 5. The tap locations were selected to match those of the nonspinning surface pressure model used in the NASA Langley tests. Some taps were offset 30 deg to the main line of taps to allow closer longitudinal spacing than could be achieved with the seal units in a single line. The taps were concentrated over the cylindrical and boattail portions of the model because the Magnus effect primarily occurs in this area. Also, the flow over the ogive including the small Magnus effect, can be analyzed quite accurately by current theoretical means. One tap was located to measure the surface pressure on the base of the model.

The operating and instrumentation wiring and tubing were routed from the model to a control console located outside the tunnel test section through a 0.875-in.-diam hole located down the length of the model sting. This hole contained the motor operating wires, motor thermocouple wires, motor cooling water tubing, scanivalve operating wires, tap engagement pneumatic pressure tubing, tap signal pressure tubing, and model bearing thermocouple wires. The water-cooled, variable frequency/variable voltage electric motor was rated at 5 hp for the nominal 4,900-rpm model spin rate. Model spin was smooth and once established, never varied more than 50 rpm from the nominal spin rate. Engagement of a pressure seal reduced the spin rate approximately 100 rpm. A photograph of the model installed in the wind tunnel test section is shown in Fig. 6.

The test procedure was first to establish the tunnel air flow at the test Mach number. The model was then set to the desired angle of attack and spun up to the test spin rate. A

| TAP NO. | TAP LOCATION Z (IN.) | Z/L | Z/d | Y (IN.) | Y (Y/d) | Θ DEG | TAP LOCATION NOTES | TAP CIRCUMFERENTIAL LOCATION WRT MAIN TAPS (DEG) |
|---|---|---|---|---|---|---|---|---|
| 1 | 22.449 | .503 | 2.824 | 3.875 | .487 | 4.5 | OGIVE | 0 |
| 2 | 23.450 | .526 | 2.950 | 3.969 | .499 | 4.5 | | 30 |
| 3 | 23.961 | .537 | 3.014 | 3.975 | .5 | 0 | OGIVE/CYLINDER JUNCTION | 0 |
| 4 | 24.461 | .548 | 3.077 | 3.975 | .5 | 0 | CYLINDER | 30 |
| 5 | 25.461 | .571 | 3.203 | 3.975 | .5 | 0 | | 0 |
| 6 | 27.461 | .615 | 3.454 | 3.975 | .5 | 0 | | |
| 7 | 29.461 | .660 | 3.706 | 3.975 | .5 | 0 | | |
| 8 | 31.461 | .705 | 3.957 | 3.975 | .5 | 0 | | |
| 9 | 33.461 | .750 | 4.209 | 3.975 | .5 | 0 | | |
| 10 | 37.821 | .848 | 4.757 | 3.975 | .5 | 0 | ROTATING BAND | 0 |
| 11 | 38.321 | .859 | 4.820 | 3.975 | .5 | 0 | | 30 |
| 12 | 38.821 | .870 | 4.883 | 3.975 | .5 | 0 | | 0 |
| 13 | 39.616 | .888 | 4.983 | 3.975 | .5 | 0 | CYLINDER | 30 |
| 14 | 40.116 | .899 | 5.046 | 3.975 | .5 | 0 | | 0 |
| 15 | 40.616 | .910 | 5.109 | 3.975 | .5 | 0 | CYLINDER/BOATTAIL JUNCTION | 30 |
| 16 | 41.151 | .922 | 5.176 | 3.938 | .495 | 7.0 | BOATTAIL | 0 |
| 17 | 42.159 | .945 | 5.303 | 3.813 | .425 | 7.0 | | 0 |
| 18 | 43.236 | .969 | 5.438 | 3.688 | .480 | 7.0 | | 30 |
| 19 | 43.725 | .980 | 5.500 | 3.625 | .456 | 7.0 | | 0 |
| 20 | 44.616 | .994 | 5.578 | 2.750 | .346 | 90° | BASE | 90 |

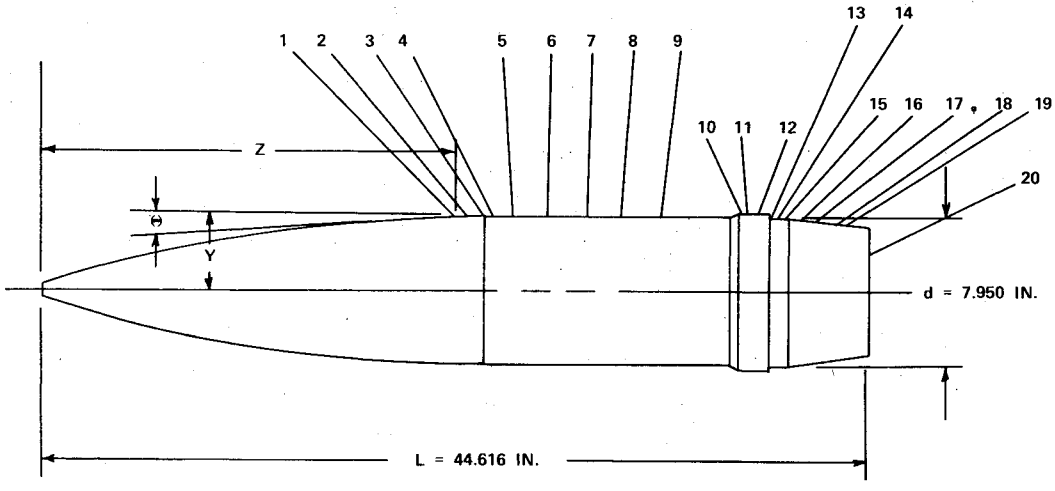


**Fig. 5 Pressure tap locations.**

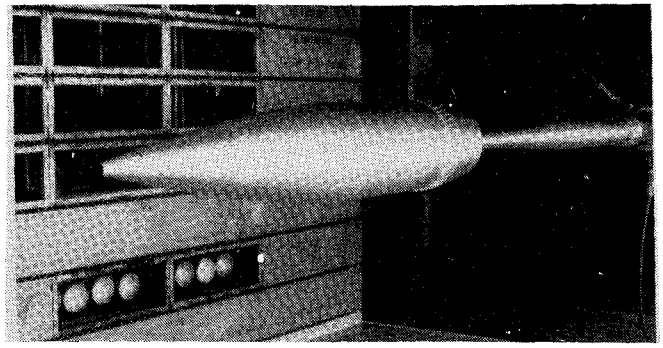

Fig. 6 Model installed in wind tunnel.

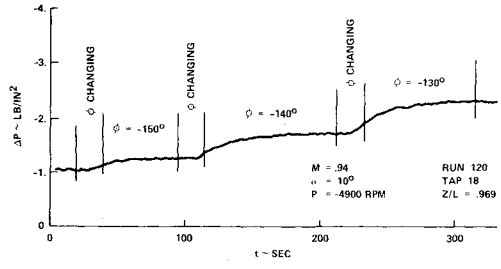


Fig. 7 Typical surface presssure measurements.

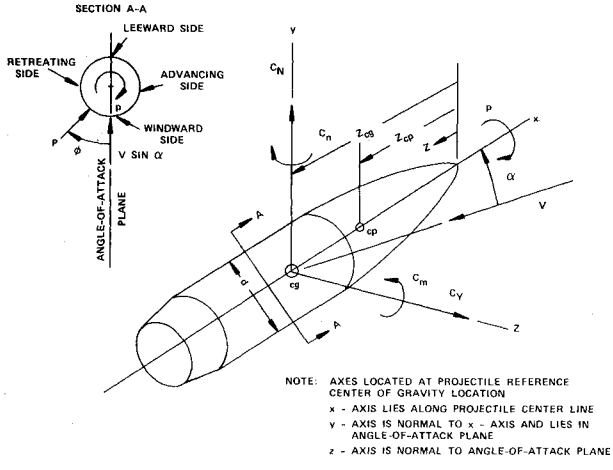


Fig. 8 Definition of terms.

single pressure tap was remotely engaged by having the scanivalve direct high-pressure air to the inner side of the seal. A pneumatic seal pressure of about 5 psi was sufficient to force the desired seal out against the inner surface of the model shell. The engaged pressure tap was then able to detect the surface pressure at that location. About 60 s were required for the measured pressure to reach its constant equilibrium value. This pressure was directed through the second scanivalve and down the model support sting via plastic tubing to a pressure transducer located outside the test section.

A special console located in the tunnel control room contained a single pressure transducer which measured the difference between the surface pressure and the test section freestream static pressure continuously displaying it as a function of time on a strip chart recorder. When the pressure was determined to be constant, the wind tunnel data system recorded the value, reduced it to pressure coefficient form, and printed it out, along with the tunnel conditions at that time. The model core was then rotated to the next circumferential position by means of the remotely controlled roll head and the procedure repeated until a complete circumferential circuit was obtained. Figure 7 presents a portion of the strip chart record. At the end of the roll circuit, the tap was disengaged, and the next tap engaged while the model was spinning. The sequence was continued until all longitudinal locations were evaluated.

After each spinning test, the model shell was removed and the O-rings changed. In most cases, the O-rings showed little or no wear. For the nonspinning tests, the model shell was locked to the core by a set screw with the vent holes aligned with their respective taps. This allowed the shell and core to be rotated together by the roll head.

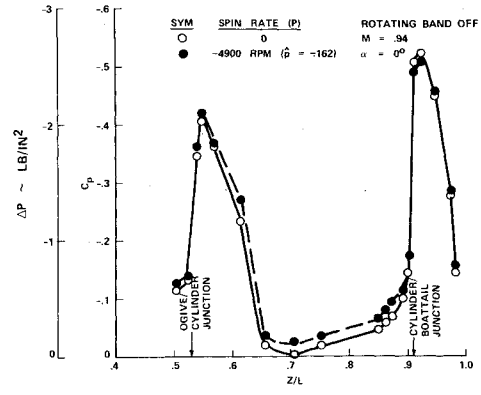


Fig. 9 Effect of spin on longitudinal surface pressure distribution for $\alpha = 0°$.

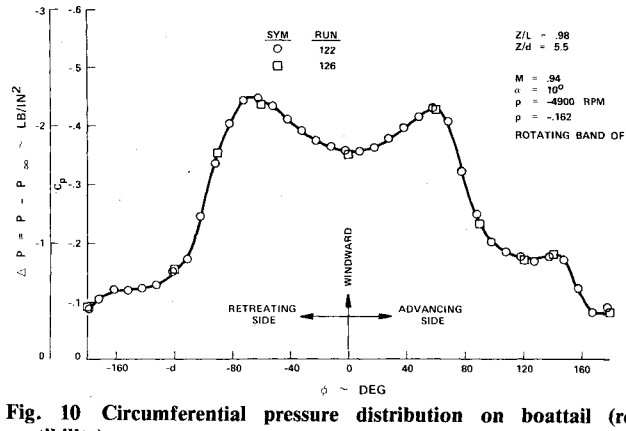


Fig. 10 Circumferential pressure distribution on boattail (repeatibility).

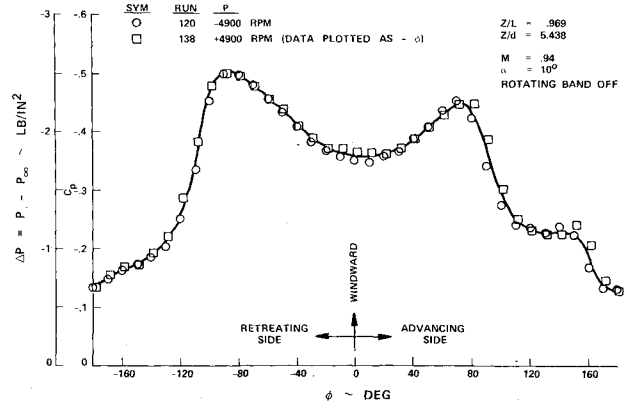


Fig. 11 Circumferential pressure distribution on boattail (symmetry).

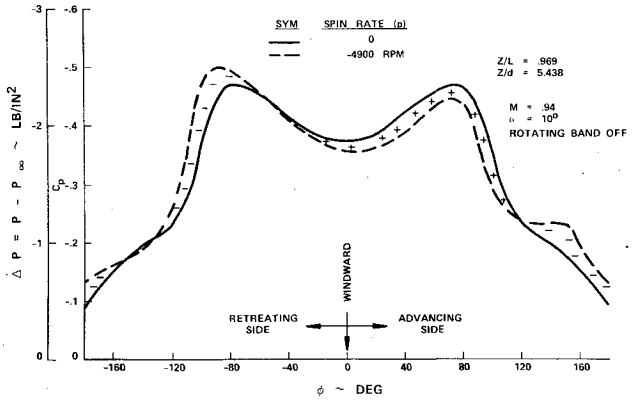


**Fig. 12 Effect of spin on boattail circumferential pressure distribution.**

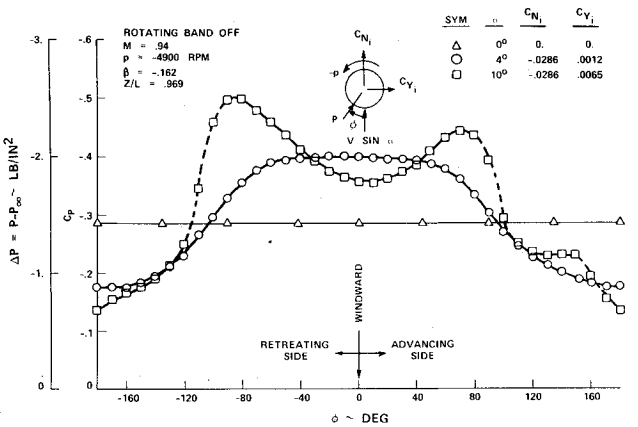


**Fig. 13 Effect of angle of attack on boattail circumferential pressure distribution.**

The long time (60 s) required for the pressure to become constant was due to the 150-ft length of tubing between the model and the transducer. This resulted in a seal engagement time of about 40 min to complete a circumferential survey at a particular longitudinal location. Over 12 h were required to test a single model configuration. Locating the transducer in the control room had several advantages, such as ease of calibration, absence of temperature effects, and providing pressure pulse damping volume. With the test method validated, future use of this technique could have the transducer located in the model or in the sector sting with a marked reduction in the tube length, pressure lag time, and consequent data acquisition time.

## Results and Discussion

The surface pressure data were reduced to coefficient form as defined in Fig. 8. Figure 9 shows the pressure measured along the projectile at zero angle of attack for both the spinning and nonspinning cases. Note that spin produces slightly reduced surface pressures at most locations. These data illustrate the ability of the testing method to measure accurately even these small pressure effects. During the test, pressure differences of 0.025 psi could be determined. The projectile base pressure measurement was essentially equal to the freestream static pressure at zero angle of attack and was not influenced by the model spin.

Figure 10 contains circumferential surface pressure data at a point on the boattail under spinning conditions. The model was spun in a counter-clockwise direction (pilot's view) in order to provide a tightening effect on the right hand threaded shell components. This negative spin resulted in a positive Magnus force. Data are shown for two separate tests and illustrate repeatability, even for the severe pressure variations

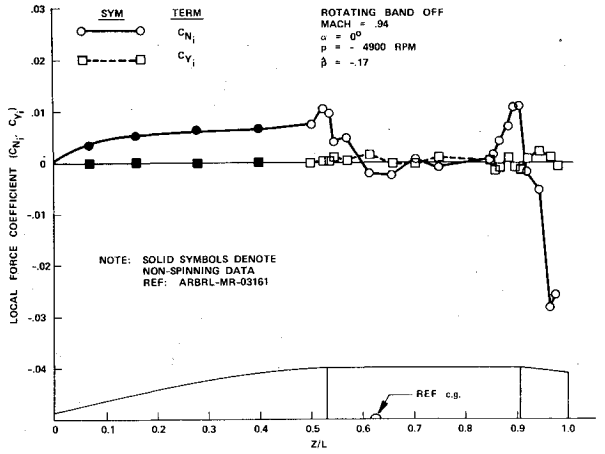


**Fig. 14 Normal and side force distribution for $\alpha = 4$ deg.**

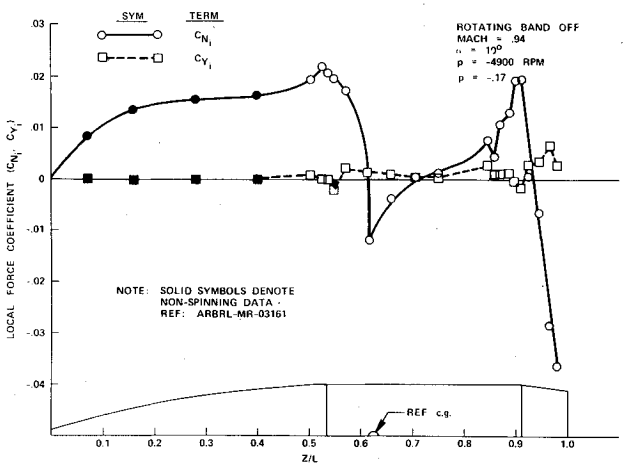


**Fig. 15 Normal and side force distribution for $\alpha = 10$ deg.**

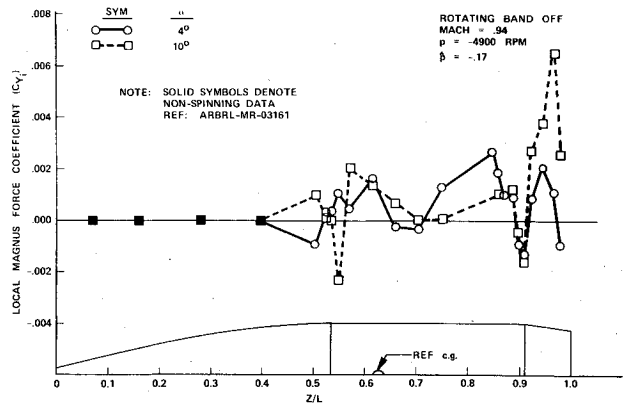


**Fig. 16 Magnus side force distribution for $\alpha = 4$ and 10 deg.**

present. Figure 11 shows similar pressure data measured on another boattail location for the model spinning in opposite directions. These data demonstrate that no asymmetric bias was present with the model or instrumentation.

The Magnus effect is clearly illustrated in Fig. 12 which shows the difference in the circumferential pressure distribution due to spin. A net negative pressure difference is produced on the retreating side of the projectile and a positive pressure difference on the advancing side resulting in an additive effect to the Magnus force. These data indicate that spin produces both a circumferential shift, as well as a distortion of the nonspinning pressure distribution.

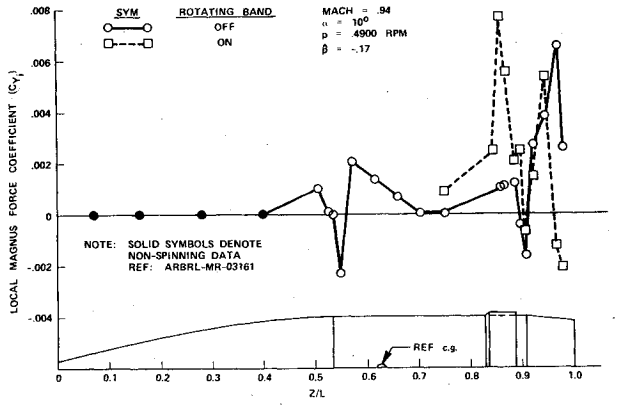


**Fig. 17 Magnus side force distribution with and without rotating band.**

**Table 1 Magnus force and moment terms for $\alpha = 4$ and 10 deg**

| | Term | $\alpha = 4$ deg | $\alpha = 10$ deg |
|---|---|---|---|
| Model configuration: | $C_{Y_p}$ (Ogive) | 0.000 | −0.004 |
| 3 Caliber ogive | $C_{Y_p}$ (Cylinder) | −0.085 | −0.092 |
| 2 Caliber cylinder | $C_{Y_p}$ (Boattail) | −0.019 | −0.080 |
| 0.5 Caliber boattail | $C_{Y_p}$ (Total) | −0.104 | −0.176 |
| Rotating band off | | | |
| $Z_{cg}/L = 0.625$ | | | |
| Test conditions: | $C_{n_p}$ (Ogive) | 0.000 | −0.003 |
| Mach 0.94 | $C_{n_p}$ (Cylinder) | 0.056 | 0.063 |
| $pd/2V = 0.162$ | $C_{n_p}$ (Boattail) | 0.033 | 0.148 |
| | $C_{n_p}$ (Total) | 0.090 | 0.208 |
| | $Z_{cp}/L$ (Magnus) | 0.779 | 0.836 |

The effect of angle of attack on the circumferential surface pressure distribution at a point on the boattail under spinning conditions is shown in Fig. 13. Note that the pressure asymmetry which produces the Magnus force is most pronounced at the largest angle of attack. The resultant local force in the angle of attack plane denoted by $CN_i$, computed by integrating the circumferential pressure distribution, does not change with angle of attack for this location. However, the resultant force normal to the angle-of-attack plane (i.e., the Magnus side force denoted by $Cy_i$) increases nonlinearly with angle of attack. These data also illustate the presence of a negative pressure "bump" on the advancing side of the leeward portion of the projectile ($\phi \cong 140$ deg). This effect is present at all longitudinal locations for the spinning projectile at $\alpha = 10$ deg, but does not occur at $\alpha = 4$ deg.

The surface pressures were integated both over the circumference and the length of the model to determine the total normal force and pitching moment and Magnus side force and yawing moment as defined in Fig. 8. The resulting normal and side force distribution along the projectile for an angle of attack of 4 deg is shown in Fig. 14 and for 10 deg in Fig. 15. As expected, the Magnus-induced side force is significantly less than the normal force in both cases. Figure 16 presents the Magnus side force at an enlarged scale.

Although a net positive Magnus force resulted for both the 4- and 10-deg angles of attack, there are longitudinal regions on the projectile where the local Magnus force acts in a negative sense. For the 10-deg case, this effect only occurs in the vicinity of the shock waves, whereas for the 4-deg case, it is also present on the cylindrical section and on the aft portion of the boattail. Note that the greatest Magnus side force occurs on the cylindrical portion of the projectile for the 4-deg case and on the boattail for the 10-deg case. A particularly large Magnus side force is present on the boattail at a 10-deg

**Table 2 Force and moment terms for spinning model with and without rotating band**

| | Term | Rotating band off | Rotating band on |
|---|---|---|---|
| Model configuration: | $C_{N_\alpha}$ (Ogive) | 1.94 | 1.95 |
| 8 in. diameter model | $C_{N_\alpha}$ (Cylinder) | 0.60 | 0.62 |
| 3 Caliber ogive | $C_{N_\alpha}$ (Boattail) | −0.31 | −0.25 |
| 2 Caliber cylinder | $C_{N_\alpha}$ (Total) | 2.24 | 2.32 |
| 0.5 Caliber boattail | | | |
| Ref. c.g. at $Z/L = 0.625$ | $C_{m_\alpha}$ (Ogive) | 3.47 | 3.47 |
| | $C_{m_\alpha}$ (Cylinder) | −0.36 | −0.39 |
| | $C_{m_\alpha}$ (Boattail) | 0.60 | 0.46 |
| Test condition: | $C_{m_\alpha}$ (Total) | 3.71 | 3.54 |
| Mach 0.94 | $Z_{cp}/L$ | | |
| $\alpha = 10°$ | | 0.33 | 0.35 |
| $R_d = 4 \times 10^6$/ft | | | |
| $p = -4900$ rpm | $C_{Y_p}$ (Ogive) | −0.004 | −0.004 |
| $\hat{p} = -0.162$ | $C_{Y_p}$ (Cylinder) | −0.092 | −0.149 |
| | $C_{Y_p}$ (Boattail) | −0.080 | −0.026 |
| | $C_{Y_p}$ (Total) | −0.176 | −0.179 |
| | $C_{n_p}$ (Ogive) | −0.003 | −0.003 |
| | $C_{n_p}$ (Cylinder) | 0.063 | 0.139 |
| | $C_{n_p}$ (Boattail) | 0.148 | 0.043 |
| | $C_{n_p}$ (Total) | 0.208 | 0.180 |
| | $Z_{cp}/L$ (Magnus) | 0.836 | 0.804 |

**Table 3 Comparison of Magnus data from surface pressure and force tests**

| | Term | Integration of surface pressure data[a] | Direct force and moment data Ref. BRLMR2284[b] |
|---|---|---|---|
| Model configuration: | $C_{Y_p}$ (Ogive) | 0.000 | – |
| 3 Caliber ogive | $C_{Y_p}$ (Cylinder) | −0.085 | – |
| 5 Caliber cylinder | $C_{Y_p}$ (Boattail) | −0.019 | – |
| 0.5 Caliber boattail | $C_Y$ (Total) | −0.104 | −0.090 |
| $Z_{cg}/L = 0.625$ | | | |
| | $C_{n_p}$ (Ogive) | 0.000 | – |
| | $C_{n_p}$ (Cylinder) | 0.056 | – |
| Test conditions: | $C_{n_p}$ (Boattail) | 0.033 | – |
| Mach 0.94 | $C_{n_p}$ (Total) | 0.090 | 0.085 |
| $\alpha = 4$ deg | | | |
| $pd/2V = 0.162$ | $Z_{cp}/L$ (Magnus) | 0.779 | 0.793 |
| | $\alpha = 4°$ | | |
| | Term | Integration of pressure surface data[b] | Direct force and moment data Ref. BRLMR2284 |
| Model configuration: | $C_{Y_p}$ (Ogive) | −0.004 | – |
| 3 Caliber ogive | $C_{Y_p}$ (Cylinder) | −0.149 | – |
| 5 Caliber cylinder | $C_{Y_p}$ (Boattail) | −0.026 | – |
| 0.5 Caliber boattail | $C_{Y_p}$ (Total) | −0.179 | −0.175 |
| $Z_{cg}/L = 0.625$ | | | |
| | $C_{n_p}$ (Ogive) | −0.003 | – |
| | $C_{n_p}$ (Cylinder) | 0.139 | – |
| Test conditions: | $C_{n_p}$ (Boattail) | 0.043 | – |
| Mach 0.04 | $C_{n_p}$ (Total) | 0.180 | 0.180 |
| $\alpha = 10$ deg | | | |
| $pd/2V = 0.162$ | $Z_{cp}$ (Magnus) | 0.804 | 0.808 |
| | $\alpha = 10°$ | | |

[a] Rotating band off. [b] Rotating band on

angle of attack. This large Magnus force, in combination with the large moment arm between the boattail and projectile center of gravity, results in a significant Magnus yawing moment. The relative contribution of the various projectile sections to the Magnus force and moment terms are summarized in Table 1 for these angles of attack.

The Magnus side force longitudinal distribution for the spinning model with the rotating band is compared to that without the rotating band in Fig. 17. The presence of the band results in a larger side force just upstream of the band, but less force downstream of the band. These compensating effects result in a similar total Magnus force and moment for the band on and band off cases. The relative contributions of the various projectile components to the Magnus terms are summarized in Table 2 for the projectile with and without a rotating band. Table 3 compares the Magnus force terms obtained from this surface pressure wind tunnel test with results from direct force and moment wind tunnel tests using scale models. In these latter tests, only the total forces and moments were measured. As can be seen, these values show good agreement.

## Conclusions

1) The sliding-seal technique is capable of accurately measuring the Magnus-induced surface pressures on a spinning projectile wind tunnel model at transonic conditions.

2) Total Magnus force and moment coefficients computed by integrating the measured surface pressure data showed good agreement with directly measured force and moment data obtained on other spinning wind tunnel models.

3) The data indicate the quantitative influence of spin and angle of attack and reveal that for a given condition, different portions of the projectile can experience both positive and negative local Magnus forces.

4) Quantitative pressure data were obtained to indicate the relative contribution of the various projectile elements (i.e., ogive, cylinder, boattail, rotating band) to the Magnus effect.

5) A significant negative pressure region was detected on the advancing leeward side of the model at all longitudinal stations for a 10-deg-angle-of-attack spinning canister. This phenomenon was not noted at a 4-deg angle of attack.

6) Model components and instrumentation functioned well; however, a pressure settling time of about 60 s was required. Future tests should have shorter pressure tubing lengths to decrease data acqusition time.

## Acknowledgments

Funding for this project was provided by the Ballistics Research Laboratory of the U.S. Army Armament, Munitions and Chemical Command and the Sandia National Laboratories.

## References

[1]Oskay, V. and Mermagen, W.H., "Transonic Flight Dynamics of Long Shell," Ballistics Research Laboratory Memorandum Rept. No. 2545, Oct. 1975.

[2]Platau, A.S. and Nielson, G.T.I., "Some Aerodynamic Characteristics of the Artillery Projectile XM549," Ballistic Research Laboratory Memorandum Rept. No. 2284, April 1973.

[3]Whyte, R.H., Burnett, J.R., Hathaway, W.H., and Brown, E.F., "Analysis of Free Flight Aerodynamic Range Data of the 155 mm M549 Projectile," Large Caliber Weapons Systems Laboratory, ARCLD-CR-80023, Oct. 1980.

[4]Kayser, L.D., Sturek, W.G., and Yanta, W.J., "Measurements in the Turbulent Boundary Layer of a Yawed, Spinning Body of Revolution at Mach 3.0 With a Laser Velocimeter and Impact Probe," AIAA Paper 78-824, July 1974.

[5]Nietubicz, C.J., Inger, G.R., and Danberg, J.E., "A Theoretical and Experimental Investigation of a Transonic Projectile Flow Field," AIAA Paper 82-0101, Jan. 1982.

[6]Kayser, L.D. and Whiton, F., "Surface Pressure Measurements on a Boattail Projectile Shape at Transonic Speeds," Ballistics Research Laboratory Memorandum Rept. ARBRL-MR-03161, March 1982.

[7]Nietubicz, C.J., Sturek, W.B., and Heavey, K.R., "Computations of Projectile Magnus Effect at Transonic Velocities," Ballistics Research Laboratory Technical Rept. ARBRL-TR-02515, Aug. 1983.

[8]Miller, M.C., "Surface Pressure Measurements on a Spinning Wind Tunnel Model," *AIAA Journal*, Vol. 14, Dec. 1976, p. 1669.

[9]Miller, M.C., "A Technique to Measure the Pressure Distribution Acting on the Surface of a Spinning Body in a Wind Tunnel," Edgewood Arsenal Technical Rept. ED-TR-76070, Sept. 1976.

[10]Miller, M.C., "Wind Tunnel Measurements of the Surface Pressure Distribution on a Spinning Magnus Rotor," *AIAA Journal of Aircraft*, Vol. 16, Dec. 1979, p. 815.

[11]Miller, M.C., "A Magnetic Fluid Seal for Measurement of Aerodynamic Surface Pressure," Chemical Systems Laboratory Technical Rept. ARCSL-TR-77018, April 1977.